QJEGH
Research article
Quarterly Journal of Engineering Geology and Hydrogeology
https://doi.org/10.1144/qjegh2025-106 | Vol. 59 | 2025 | qjegh2025-106

Multiphysical monitoring of a thermal plume during mine water geothermal experimentation

Andres Gonzalez Quiros[1]*, Alison Monaghan[1], Mylene Receveur[1], Paul Wilkinson[2], David Boon[2], Kyle Walker-Verkuil[1], Vanessa Starcher[1], Donald John MacAllister[1] and Oliver Kuras[2]

[1] British Geological Survey, Edinburgh, UK
[2] British Geological Survey, Nottingham, UK
AGQ, 0000-0003-1102-8626; AM, 0000-0003-2147-9607; MR, 0000-0002-8481-0478; PW, 0000-0001-6215-6535; DB, 0000-0003-4921-8249; KW-V, 0009-0007-0835-0418; DJM, 0000-0001-8893-9634; OK, 0000-0003-2623-1635
* Correspondence: aquiros@bgs.ac.uk

Abstract: The rate and magnitude of conductive and advective thermal processes that control the efficiency and sustainability of mine water geothermal and thermal energy storage are poorly quantified. We present results of multiphysical observations collected during a 25-day heat extraction experiment performed on an abstraction–reinjection mine water well doublet at the UK Geoenergy Observatory in Glasgow. The results showed how the thermal plume generated by injection of cool water developed from the injection borehole, mainly driven by advection at the level of mine workings. Heat conduction around the cased part of the injection borehole resulted in different cooling rates related to lithological variations, clearly shown in the distribute temperature sensing data. The electrical resistivity tomography monitoring provided a time-lapse image of the evolution of the cool plume, which extended laterally within the mine workings to pass a borehole located at 10 m away in less than 2 days, and later above the mine workings into the bedrock. It also showed how the effects of cooling remained for at least 18 days after the injection stopped, providing new insight into thermal storage behaviour of mine water systems. The results provide an unprecedented opportunity to visualize the effects of geothermal operation in mine water settings and are useful guidance for project developers and regulators.

Thematic collection: This article is part of the Mine Water Energy collection available at: https://www.lyellcollection.org/topic/collections/mine-water-energy

Received 16 July 2025; **revised** 24 October 2025; **accepted** 4 November 2025

Mine water geothermal and thermal energy storage in flooded mines are attractive options to help decarbonize the heating and cooling demand of buildings (Chu *et al.* 2021), especially in post-mining regions that are the focus of regeneration and reindustrialization efforts. The technology has been proved, with operational schemes in various countries (Canada, Spain, Netherlands, UK) (Jessop *et al.* 1995; Jardón *et al.* 2013; Verhoeven *et al.* 2014; Walls *et al.* 2021).

One of the key technical uncertainties that affects the efficiency and sustainability of mine water geothermal projects is understanding the rates and magnitude of the thermal processes, including the heat transport via conduction in the rock mass and the extent and evolution of a thermal plume driven by advection (e.g. Lesparre *et al.* 2019). These are, however, very relevant to understand and/or predict key characteristics for a satisfactory geothermal operation. Among them, estimating the theoretical available geothermal heat (e.g. Ciriaco *et al.* 2020) and/or storage potentials (e.g. Hahn 2024), the volume of influence of the operation and potential hydraulic and/or thermal interferences (e.g. Bloemendal *et al.* 2014; Sweeney *et al.* 2025), the ratios of energy exchange and performance (e.g. Cai *et al.* 2021) or the early detection or observation of thermal breakthrough (e.g. Fadel *et al.* 2022).

The field observation of these processes is mostly limited by the restricted direct access to the subsurface after the mines were closed and flooded. Monitoring access is only possible at old mine entrances, such as adits or shafts, or through existing or newly drilled boreholes targeted to specific locations in the system. These are usually sparse and not able to provide a full assessment and understanding of the flow pathways and temperature variations in the complex and heterogeneous mine-aquifer system.

An advanced and alternative approach is to use and combine multiple techniques to collect both direct (e.g. downhole loggers) and indirect (e.g. geophysics) information of the variables and properties of interest, with different levels of resolution (e.g. Comte *et al.* 2017). The indirect methods provide additional information of the hydraulic and thermal processes of the rock mass at a different spatial and temporal scale, they are able to provide two- and three-dimensional images of the extent and volume affected by the geothermal operation and can be used for parameter identification and estimation combined with multiphysical mathematical modelling (e.g. Binley *et al.* 2015).

In this work we present the results of multiphysical monitoring of a heat abstraction experiment at the UK Geoenergy Observatory (UKGEOS), in Glasgow (Scotland, UK), an at-scale research site equipped with geothermal infrastructure and state-of-the-art monitoring capabilities built to derisk the development of mine water geothermal and thermal energy storage (Monaghan *et al.* 2022). The combination of measurements from downhole loggers and surface sensors, electrical resistivity tomography (ERT) and fibre-optics distributed temperature sensing (DTS) has enabled for a more detailed characterization of the subsurface and a better understanding of the hydraulic and thermal processes under both natural conditions and during a geothermal heat-extraction experiment. This level of detailed monitoring, which is usually neither possible nor realistic in most operational schemes, provides a unique opportunity to increase the understanding of the processes and role of hydraulic and thermal properties at the scale of operation. These learnings can be transferred to similar systems in the UK and worldwide, and be used by developers, designers, operators and regulators for sustainable and efficient management

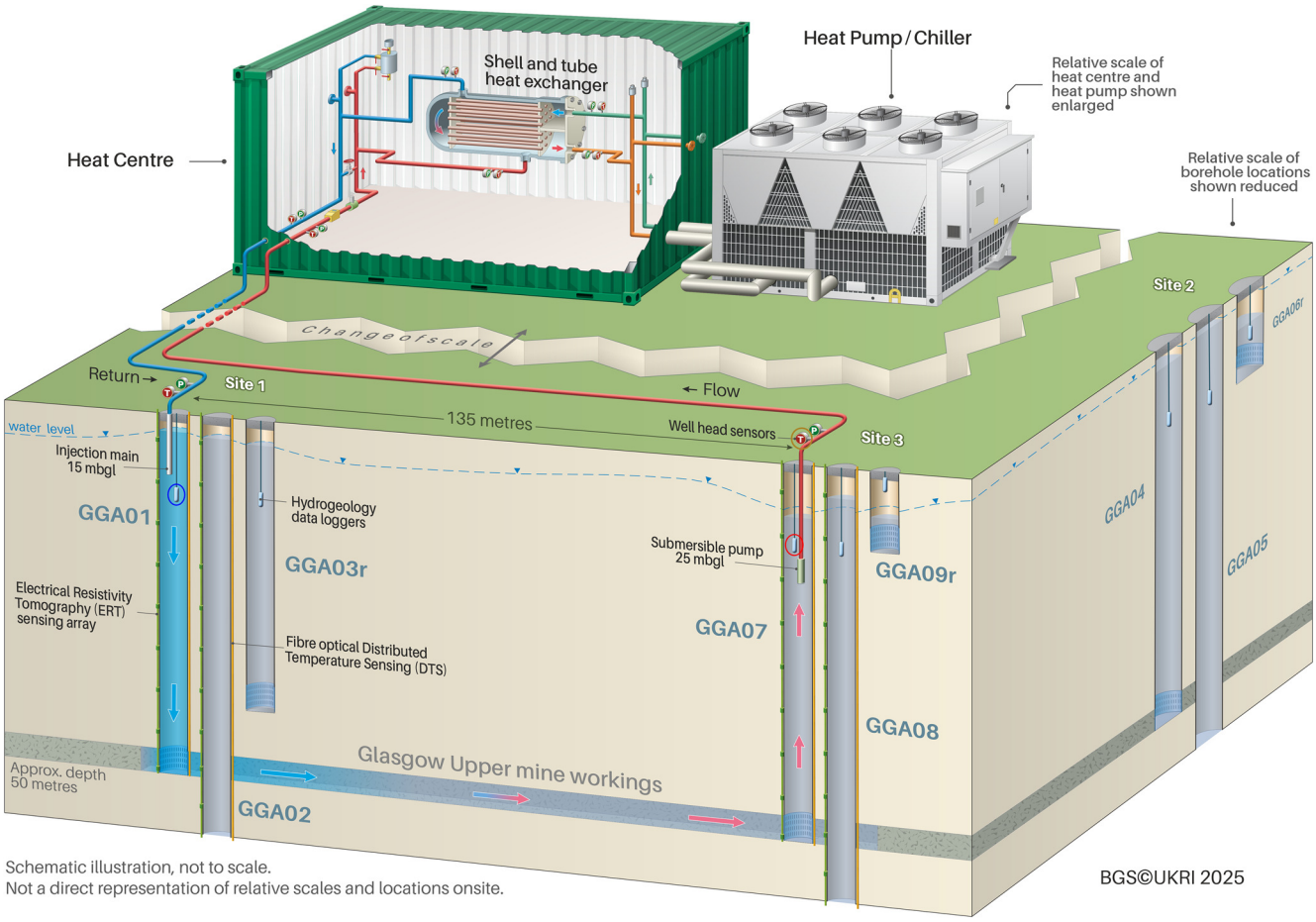

Fig. 1. Geothermal and monitoring infrastructure of the UK Geoenergy Observatory in Glasgow used in the experiment. Circles show the downhole loggers (GGA01, GGA07) and well head sensor (GGA07) presented in Figure 2. A full diagram including the Glasgow Main and the complete infrastructure (including all heat exchangers and pipes) is available at www.ukgeos.ac.uk.

of mine water geothermal and mine thermal energy storage (MTES) systems, the optimization of monitoring networks and for the development and application of specific regulation.

Methods

UK Geoenergy Observatory, Glasgow

General context

The UK Geoenergy Observatory is an at-scale research facility located in the Cuningar Loop Woodland park (Grid Ref: NS 62255 62870) in the SE of Glasgow (Scotland, UK). The Observatory is a unique experimentation site equipped with geothermal and monitoring infrastructure for research and innovation related to mine water geothermal and thermal energy storage (Monaghan *et al.* 2022; https://www.ukgeos.ac.uk/).

The Observatory is located in the Central Coalfield of the Midland Valley of Scotland. The geology consists of the Scottish Coal Measures Group (Upper Carboniferous), comprising cyclical sequences of sandstone, siltstone, mudstone, root-bearing palaeosol ('seatearth') and coal (Hall *et al.* 1998).

The mine workings intersected by the Observatory boreholes exploited coal from the Glasgow Upper (GU), Glasgow Ell and Glasgow Main (GMA) coal seams (Westphalian B) (Monaghan *et al.* 2022). The most common mining method in these mines was 'pillar and stall' (also called 'stoop and room' or 'room and pillar'). Mine working plans show irregular distribution of the stalls. Some areas were later transformed to total extraction zones, in which the weight-bearing coal pillars were removed. After mining, these zones are characterized by variable conditions, including open voids, rubble zones ('goaf') after collapse of the roof or backfilling of the voids with packed or loose mine waste (Monaghan *et al.* 2022). Overlying the Carboniferous sequence there is a heterogeneous sequence of superficial Quaternary deposits of variable thickness and composition, accumulated mainly along the Clyde River valley (Ó Dochartaigh *et al.* 2019).

The mine workings have a predominant role in the hydrogeological processes in the Carboniferous aquifer after mine closure and groundwater rebound. The hydraulic heads are higher in the Glasgow Main (the deeper mine workings) than in the Glasgow Upper and in the superficial aquifer, confirming an upwards hydraulic gradient (Gonzalez Quiros *et al.* 2024). The mined zones have high transmissivities, with very good lateral (horizontal) connectivity. Water level monitoring data and pumping tests have shown that the vertical connectivity between the Glasgow Main, Glasgow Upper and the superficial aquifers is very limited. Temperatures are slightly higher in the Glasgow Main (~12.5°C) than in the Glasgow Upper (~11.95°C) mine workings.

Geothermal infrastructure

The geothermal infrastructure links four boreholes (GGA01, GGA07, GGA05 and GGA08) via buried pipework into a small heat centre (Fig. 1). Each of the four boreholes, two screened at each mine interval (GGA01 and GGA07 at the Glasgow Upper, and GGA05 and GGA08 at the Glasgow Main), are designed to be used in either abstraction or injection mode but, currently, Grundfos SP

46-6 submersible pumps for abstraction are only installed at 25 mbgl in GGA07 and GGA05. The 9.2 kW rated pumps operate at flow rates for the mine water side of 3–12 l s^{-1}. The injection mains are installed at 15 mbgl in GGA01, GGA05, GGA07 and GGA08.

The heat centre contains three heat exchangers (shell and tube, stainless steel plate and brazed plate) to evaluate and compare their performance under operational conditions as they have different heat transfer coefficients and maintenance requirements. They operate independently and are coupled to a 200 kW peak capacity reversible air to water heat pump/chiller unit using a 30% glycol fluid in the intermediate closed loop circuit. The system can operate in either a heat extraction mode (taking heat from the mine water) or in a heat injection mode (adding heat into the mines).

In-line sensors are installed across the system to measure circulation water pressure, temperature and electrical conductivity. These can be used in conjunction with the downhole hydrogeological data loggers to obtain information about subsurface and surface changes (Fig. 1).

Fibre optics – distributed temperature sensing

Fibre-optical distributed temperature sensing (FO-DTS) cables were installed in the boreholes that intersect the mine workings. The FO-DTS cables were attached to the outside of the PVC casing and are only in direct contact with the mine water at the depths of the screened intervals. In the rest of the borehole, grout was used to fill the annular space between the casing (and cable attached to it) and the rock (Monaghan *et al.* 2020*a*, *b*) (i.e. cables are encased in cement grout and have good thermal coupling with the bedrock). An exception in the FO installation and data collection at the Glasgow Upper interval in borehole GGA02. A grout plug was used to seal the Glasgow Upper mine working during construction of the borehole and this grout has penetrated further into the mine working than the downhole annulus grout in which the fibre-optical cable was cemented (Monaghan *et al.* 2020*b*). The FO-DTS cables are in double-ended configuration, except GGA02 which is single ended.

The Silixa XT interrogators set to measure for 60 s duration every 10 minutes and resolve ~0.01°C temperature measurements at 0.254 m spacing down the borehole. For interpretation, length along fibre (LAF) measurements were filtered and converted into time–depth profiles, removing sections of the cable at the surface between the borehole top and the DTS interrogator unit. Final datasets were compiled and presented as depth–temperature profiles to show the temporal evolution of temperatures along the borehole before, during and after the heat extraction period.

Electrical resistivity

Along with the fibre optic cables, linear arrays of electrodes were attached to the outside of the casings on boreholes GGA01, GGA02, GGA04, GGA05, GGA07 & GGA08. The electrodes were 15 mm diameter stainless steel tubes with exposed lengths of 100 mm, spaced at 0.75 m intervals. Boreholes GGA02, GGA05 & GGA08 had 72 electrodes each extending between *c.* 35 and 90 mbgl (spanning the Glasgow Upper and Glasgow Main mine workings) and boreholes GGA01, GGA04 & GGA07 had 24 electrodes each between *c.* 35 and 55 mbgl (spanning the Glasgow Upper mine workings only). Some electrodes were not usable due to either the presence of metallic casing or damage during installation.

Each of the electrode arrays is connected to a BGS PRIME ERT monitoring system (Holmes *et al.* 2020). These permit flexible scheduling of arbitrary measurement schemes at the user's control. During commissioning it was noted that measurement configurations with predominantly sub-horizontal current flow (e.g. cross-hole configurations) produced notably different inverse images to those with predominantly sub-vertical current flow (e.g. in-hole configurations). The source of these discrepancies is still under investigation, but electrical anisotropy is suspected to be the primary cause. To minimize the effects of anisotropy on the predominantly isotropic inversion algorithms that are widely available, measurements for this experiment were restricted to in-hole configurations. The dipole-dipole type was chosen due to its superior image resolution, using dipole lengths of $a = 0.75$–17.25 m (1–23 electrode spacings) and inter-dipole spacings of $n{\cdot}a$ where $n = 1$–7. Reciprocal measurements were also made to assess data quality, with the reciprocal error estimate taken as the standard error in the mean of the reciprocal data pair. Dipole–dipole measurements make efficient use of multichannel instruments, enabling the PRIME system to measure full sets of reciprocal dipole–dipole data as rapidly as every 30 minutes.

The data were assessed for quality, removing any involving non-functional electrodes, any with negative apparent resistivities, and any with reciprocal errors >5%. The reciprocal error estimates were modelled as a quadratic function of the transfer resistance and used to weight the data in the inversion. The inversion was carried out using a Gauss–Newton least-squares method as implemented in the freeware code R3t (Binley and Slater 2020) using a structured triangular prism mesh to allow for anisotropic L2-norm smoothness constraints to be applied with a ratio of 4:1 smoothness in the horizontal compared to the vertical direction. This was chosen to reflect the expected horizontally layered nature of the lithology and mine workings. Time-lapse models were then produced during the experiment using the difference inversion method of LaBrecque and Yang (2001).

Geothermal experiment

A 25-day heat extraction experiment was performed at the end of 2023 (started on the 28 November and pumps were stopped on 22 December) to test the geothermal infrastructure and monitoring capabilities. The test consisted of a continuous mine water abstraction from GGA07 and reinjection of cooled water in GGA01 (Fig. 1), both screened in the Glasgow Upper mine workings, at a flow rate of 6 l s^{-1}.

The abstracted water, at a temperature of between 11.9 and 12.0°C, was reinjected after removal of between 3 and 4°C (Fig. 2) via the shell and tube heat exchanger (Fig. 1). Surface pressure and temperature sensors, downhole hydrogeology loggers, FO-DTS and ERT monitored for the duration of the heat abstraction test and during a period of post-cooling recovery of approximately two and a half weeks until 9 January 2024.

Several experiments of various lengths were run in the Observatory in the previous months. A heat injection experiment performed at the Observatory in September 2023 (Gonzalez Quiros *et al.* 2025), using the same configuration of boreholes (abstraction at GGA07 and re-injection in GGA01) with a 12 l s^{-1} flow rate, resulted in a thermal breakthrough (temperature change of more than 0.1°C) at the abstraction borehole GGA07 after 116 hours (i.e. less than 5 days). At the end of the heat injection (average temperature 17.4°C) experiment that ran for 17 days the temperature at the abstraction borehole was 12.5°C, which was 0.6°C higher than the initial temperature. In the injection borehole a gradual drop in the temperature was observed for weeks at the mine workings level, with a final DTS measurement of 13.4°C at the screen level seven weeks after the end of the heat injection, just before a one-day cool injection experiment on 16 November disturbed the heat plume generated in September.

Results

Temperature monitoring

Figure 2a shows the abstraction and reinjection temperatures measured during the experiment and part of the recovery phase.

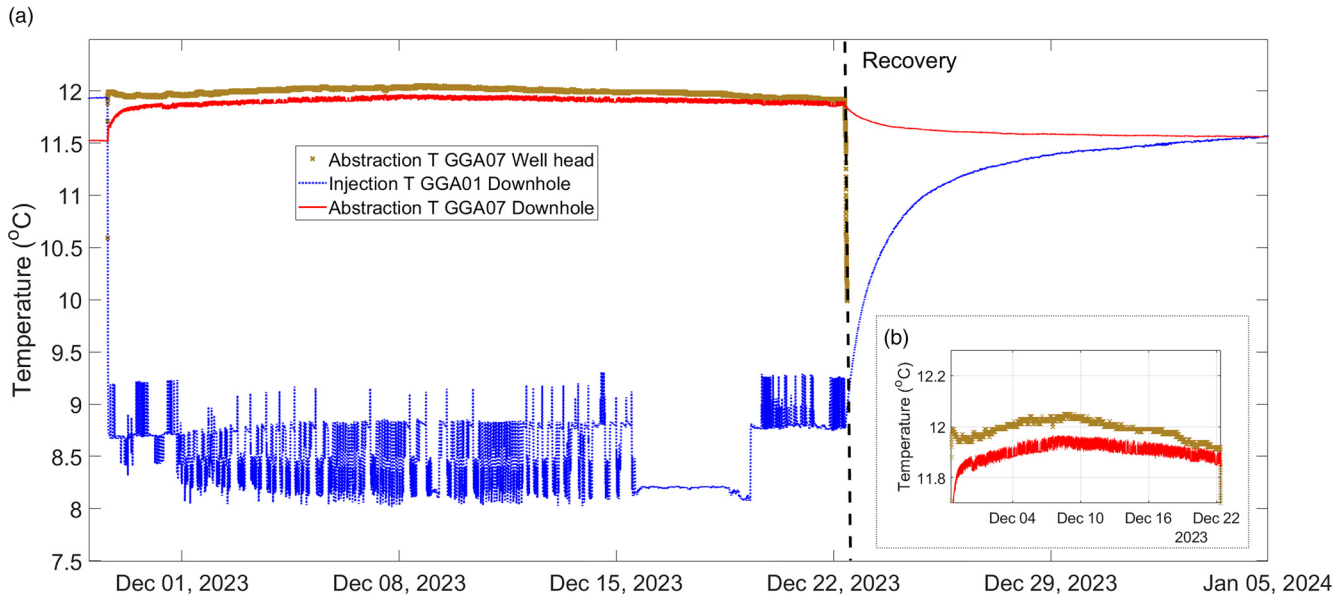

Fig. 2. (**a**) Temperature v. time data from the injection borehole GGA01 (downhole logger, blue line) and the abstraction borehole GGA07(downhole logger, red line; well head sensor, yellow markers) during the experiment. Well head data are not shown for the recovery as they are influenced by ambient temperature. (**b**) Inset is a zoomed image showing in more detail the temperatures at the abstraction borehole GGA07 (recovery period not included).

The average injection temperature of 8.61°C, with maximum of up to 10.44°C and minimum of 7.04°C were measured at short intervals due to fluctuations caused by the heat pump/chiller. On average this is 3.38°C cooler than the temperature at the start (i.e. the average ΔT of the heat extraction), with minimum of 2.51°C and maximum of 3.92°C. During the most stable period of injection between 16 and 20 December the ΔT was approximately 3.7–3.8°C. The temperatures measured in both the wellhead sensor and the downhole logger in GGA01 were very similar, reflecting the location of the downhole logger (−12.3 metres above OD (maOD)) below the reinjection main (−4.7 maOD) (GGA01 logger temperatures are not shown in Fig. 2a). Different periods or trends in the injection temperature were identified due to the performance of the heat pump/chiller. Two unstable periods were observed: between the start of the experiment and 15 December, and between 19 December and the end of the test. Both with an average injection temperature that ranged between 8.7 and 8.9°C and short fluctuations with changes of −0.8°C and +1.5°C with respect to the average. Between 16 and 20 December, a more settled temperature of 8.2–8.3°C was observed, with no visible fluctuations of more than 0.1°C. This coincided with four days when the outdoor air temperature was consistently higher than the injection temperature.

The abstraction temperature measured in the pumped water stream at the well head in GGA07, located at a horizontal distance of 135 m from the injection well, represents the mine water temperature (plus a small amount of heat from the pump) as it measures water being pumped up the borehole and passing the sensor at a rate of 6 l s^{-1}. The temperature at this point, which with no Observatory operation reflects ambient conditions at the surface, increased almost instantaneously as soon as abstraction started. It fluctuated in the first hours of the experiment, decreasing from 11.99°C to 11.94°C. After two days of the heat extraction period, it started to increase and reached a maximum 12.05°C at the end of 8 December. From that day, temperature decreased constantly and reached 11.91°C at the end of the abstraction on 22 December. The downhole logger gave slightly different measurements to the well head sensor in GGA07 (Fig. 2b), resulting from the position of the logger (−9.8 maOD) a few metres above the submersible pump (−13.4 maOD) and abstraction main. We interpreted this minor temperature shift as being due to borehole effects, including the relative vertical movement of the water column caused by the drop of water level after pumping starts and water circulation inside the borehole caused by the operation of the submersible pump. The downhole logger had an initial temperature of 11.65°C, which steeply increased in temperature until it reached a temperature of around 11.85°C two days after the abstraction started. Then the temperature increased with a similar trend as the well head sensor, reaching a maximum of around 11.95°C on 8 December, approximately 0.1°C lower than the temperature measured at the well head sensor at the same time. After that day, there was a continuous decrease of temperature but with a less steep gradient than in the well head until it reached 11.87°C at the end of the experiment (0.05°C lower than the well head).

Groundwater monitoring

Figure 3 shows the groundwater levels (maOD) measured in the three Glasgow Upper boreholes (GGA01, GGA04 and GGA07) during the experiment. Before the pumps were on, the groundwater levels at the GU boreholes were ∼9.3 maOD, while in the Glasgow Main boreholes, the deeper mine workings, were ∼10.3 maOD, which is around 1 m higher.

At the start of the experiment, the abstraction borehole (GGA07) suffered a drawdown of about 0.2 m, while in the reinjection borehole GGA01 the increase in groundwater levels was about 0.04 m. This illustrates the higher transmissivity of the mine workings that has been previously documented around borehole GGA01 (Shorter *et al.* 2021; Gonzalez Quiros *et al.* 2024). The groundwater levels in GGA04, located at approximately the same distance from the abstraction and injection boreholes, and GGA03r, screened in the bedrock above the GU mine working about 20 m away from GGA01, remained unaffected by the experiment. Overall, no changes were observed in the groundwater levels in the Glasgow Main mine working during the experiment in the shallower Glasgow Upper.

Over the duration of the experiment, natural fluctuations caused by barometric pressure changes and precipitation events led to groundwater level variations of up to 0.5 m in all the GU mine boreholes (Fig. 3), typical of the previously observed baseline variations (Gonzalez Quiros *et al.* 2024). Groundwater levels

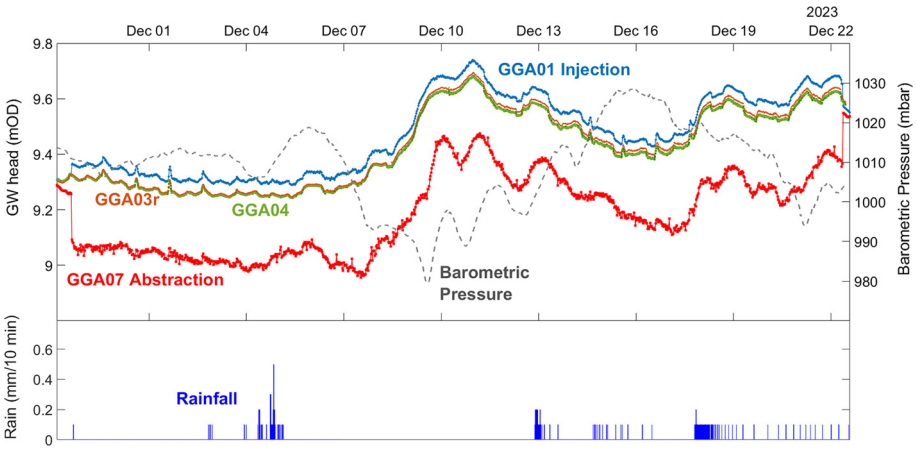

Fig. 3. Groundwater data from the three Glasgow Upper mine boreholes (GGA01, GGA04 and GGA07) and the bedrock borehole GGA03r during the test with barometric data (dashed line/scale on right-hand side) and precipitation) data (blue graph, scale on left-hand side). GW Head, groundwater head.

reached their maximum on 10 December, during a period of lower pressures, increasing to 9.74 mAOD in GGA01 (i.e. more than 0.4 m increase compared to initial groundwater levels) and 9.47 mAOD in the abstraction borehole GGA07. Groundwater levels in the abstraction borehole GGA07 increased in these days to values higher than the initial groundwater level, showing that natural changes can be, under some conditions, of higher magnitude than those caused by geothermal operation (at 6 l s^{-1} in this experiment). Increase in groundwater head of lower magnitude was also observed after rainfall events, especially on 6, 13 and 18 December. GU Boreholes GGA01 and GGA04 responded similarly to these natural changes, while GGA07 showed slightly higher amplitudes after both precipitation events and atmospheric changes than the other two GU boreholes.

Distributed temperature sensing

Temperature profiles extracted from DTS data acquired in the mine water boreholes before the start of the experiment show an apparent geothermal gradient (below the zone of seasonal fluctuation) of approximately 12°C km^{-1}. A year of monthly depth–temperature records (average surface temperature of 11°C) from GGA08, screened at the Glasgow Main and located 10 m apart from the abstraction borehole GGA07, and not as largely impacted by geothermal experiments, is shown in Figure 4a. The natural variations in the near-surface temperature due to seasonal fluctuations in air temperature are observed in all four boreholes down to *c.* 9 m below ground level. DTS near-surface temperatures correlate well with the temperature measured at the weather station at Site 1 in

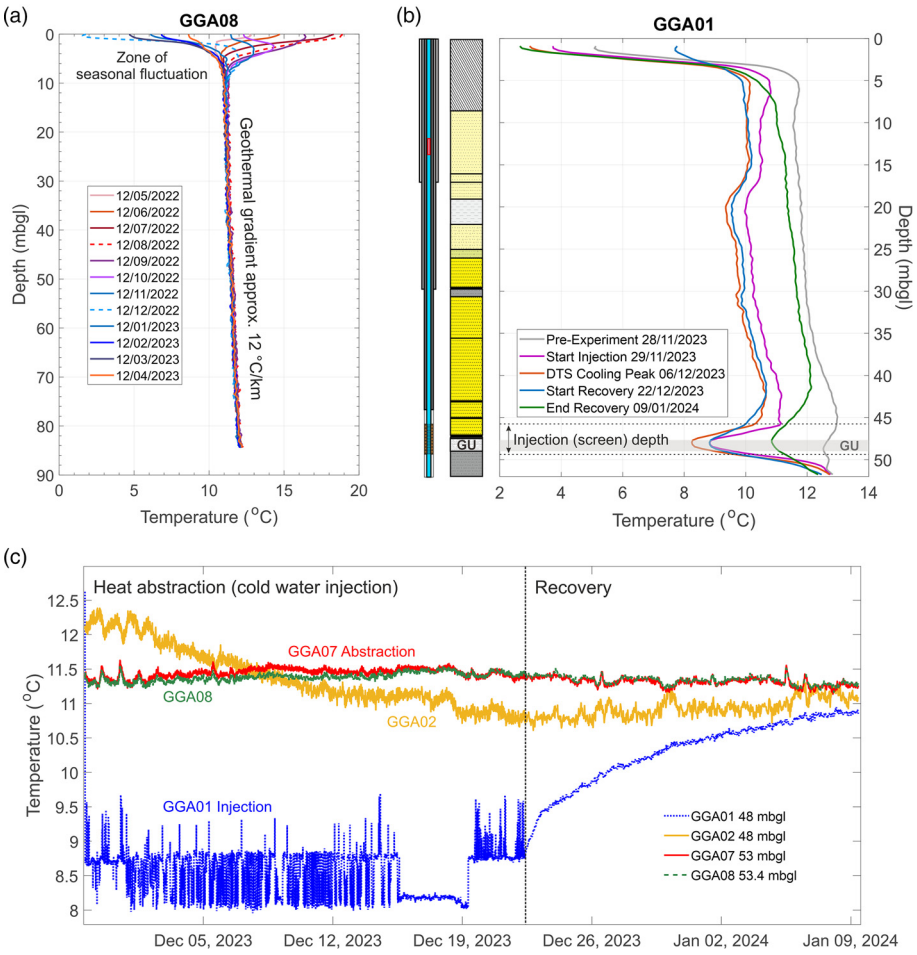

Fig. 4. (**a**) Baseline temperature in GGA08 showing the geothermal gradient undisturbed by any experiment and the effect of seasonal fluctuations in the upper *c.* 10 m below ground level. (**b**) DTS profiles at selected times (before, during the experiment and during recovery) in the injection borehole (GGA01), borehole construction, geological log and location of the screened interval and Glasgow Upper (grey shading) are shown for reference (Fig. 5 for details). (**c**) Temperature time-series measured by the DTS at the GU depth in the four mine boreholes (in GGA02 the cable is not in direct contact with mine water and GGA08 is not screened at GU).

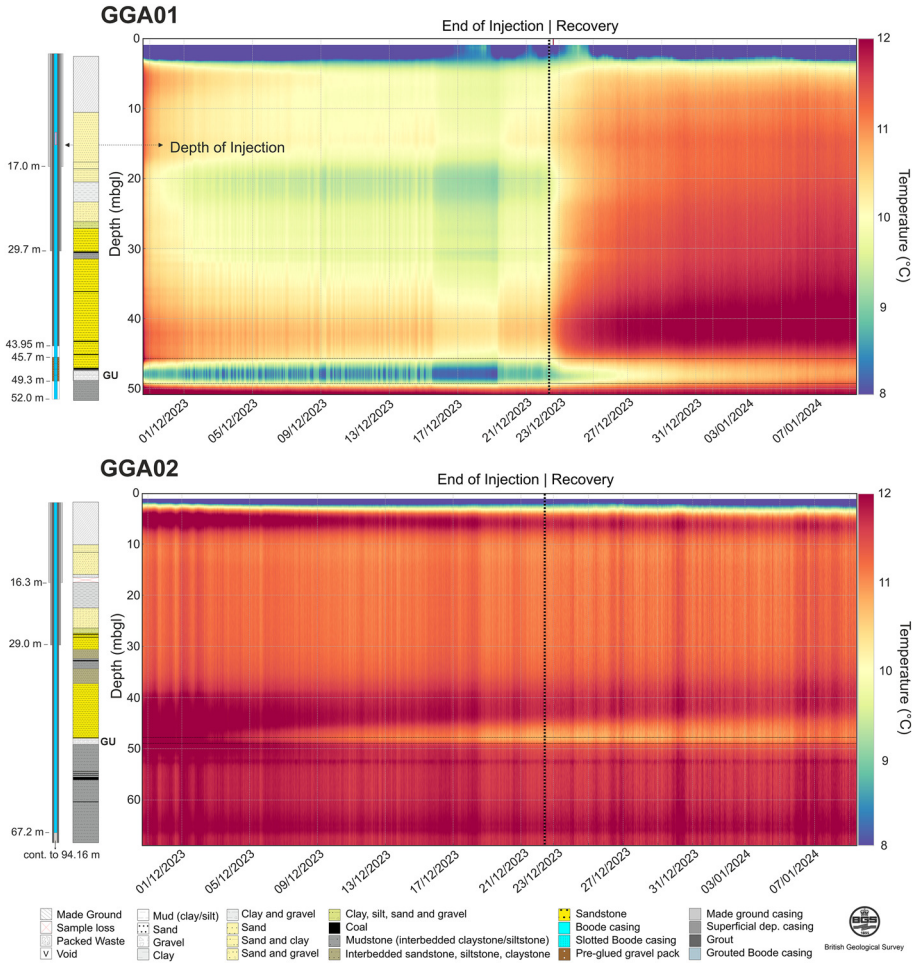

Fig. 5. DTS time–depth sections for GGA01 (upper) and GGA02 (lower) during the heat abstraction and recovery experiment. The geological log and borehole construction details are shown for reference.

the Cuningar Loop, and the depth–temperatures with the initial temperature measured in the downhole loggers (i.e. not reflecting the mine water temperature but the equilibrium temperature of the water column in the borehole at the logger depth).

The DTS data reveal, with an unprecedented level of detail in mine water geothermal applications, the induced changes in temperature down the borehole and at the level of mine workings caused by the injection of cooled mine water. During the experiment, the injection of cooler water in GGA01 was observed in the DTS data as a rapid and relatively uniform cooling along the borehole (Figs 4b, 5). Horizontal bands in Figure 5 show the variable rates of temperature change and reflect the variation of thermal properties with depth, linked either to lithological changes and/or borehole construction. A clearly visible cooler band at *c.* 30 mbgl is aligned with a mudstone layer, where temperature decreased from 12.03°C at the start of the injection on 28 November down to 9.87°C at the end of the injection on 22 December, while a warmer horizon was observed at the sandstone depth between *c.* 40 and 45 mbgl, with temperature at this level decreasing from 12.79°C at the start of the injection to 10.24°C at the end of the injection. The cooling was more pronounced below *c.* 16 mbgl, which coincides with the location of the injection main and, especially, at the level of the clay (Paisley Clay member) at *c.* 20 mbgl. At this level the temperature decreased from the initial 11.84°C to 9.68°C on 22 December. This point also reached the lowest temperature in the cased section during the experiment, 9.21°C on 19 December (Fig. 4b). In the screened interval, between *c.* 45 and 49 mbgl, where the fibre optic cable is in direct contact with the injected mine water at the depth of the Glasgow Upper mine workings, a 'cool' horizon extended from the start to the end of the injection period. The injected water temperature fluctuations between 8 and 9°C measured in the wellhead sensor (Fig. 2) were also measured by the DTS during the experiment and are observable in the DTS time-series from the GU interval in GGA01 (blue curve in Fig. 4c), and along the fully cased (non-screened) interval in GGA01 shown as vertical bands of temperature changes in Figure 5, particularly noticeable at the mine working level with the period of more stable temperatures observed between 16 and 20 December.

The cessation of injection resulted in a quick temperature recovery in the cased section of the GGA01 borehole (Fig. 5). However, temperature profiles extracted at different times in GGA01 (Fig. 4b) suggested the persistence of a thermal footprint at the end of the recovery period, with the average temperature along the borehole being *c.* 1°C lower than before the start of the experiment. Key characteristics obtained from the DTS are summarized below.

- The pre-experiment profile is likely to record residual thermal disturbances from previous experiments. Mainly a 3-week heat injection experiments that finished in October 2023 and various shorter (less than 1 hour-long) cool injection experiments in November 2023, and therefore does not represent the absolute undisturbed baseline temperature, especially at the depth of the Glasgow Upper mine workings.
- The rate of cooling is higher (lower temperatures observed) at the clay (*c.* 20 m depth) and mudstone (*c.* 30 m depth) intervals, compared to the sandstone intervals.
- At the end of the recovery period considered in this work (9 January) the temperature was still lower than the initial temperature before the start of the experiment: 0.32°C lower at 20 mbgl (clay), 0.3°C lower at 30 mbgl (mudstone) and 0.74°C lower at 40 mbgl (sandstone).

- The temperature recovery was much lower at the depth of the Glasgow Upper mine workings, it increased from 8.75°C at the end of the injection to 10.91°C at the end of the reported recovery period, which still was 1.67°C lower than the initial 12.58°C measured at the start of the experiment on 28 November.

During both injection and the subsequent recovery period, the GGA01 DTS data show the progressive vertical dissipation of heat (i.e. above and below the mine workings) during recovery, especially above the screened interval (Fig. 5). As the recovery period extends, the amplitude of the cool signal visible on the temperature profiles at the GU interval becomes wider vertically but smoother (Fig. 4b). This has been interpreted as the relative cooling via conduction through the sandstone roof above the GU mine working.

In GGA02, 10 m from GGA01 and in between it and the abstraction borehole, the DTS data (Fig. 5b) showed a decrease of temperature at the depth of the GU mine workings after approximately 3 days. GGA02 is a fully cased borehole drilled through a thicker grout plug at that depth. Hence, the DTS cable is not in direct contact with the GU mine water and the signal recorded might not represent the true arrival of the 'cool' water in GGA02, as conduction through the grout plug might delay the detection of the thermal plume. GGA02, contrary to GGA01, does not show a clear temperature increase (recovery) after the end of the experiment and during the recovery period (Figs 4c, 5b).

In the abstraction borehole, GGA07, a small temperature increase of up to 0.3°C was observed in the DTS at the GU mine working interval since the start of the experiment and until 9 December (Fig. 4c), 11 days after the start of pumping. From 9 December, similar to what was observed in the downhole and well head temperature loggers (Fig. 2), the temperature in GGA07 started decreasing by less than 0.2°C after 13 days of pumping, that is a similar magnitude compared to the change measured in both the downhole and wellhead loggers. In GGA08 the increase, and later decrease in temperature was more attenuated, but at the end of the experiment both GGA07 and GGA08, 10 m apart, showed very similar temperatures. These observations are interpreted as a pulse of heat from a previous heat injection test (shown as remnant heat with warmer water in the GU pre-experiment profiles in the injection borehole GGA01 in Fig. 4b) and the subsequent arrival after 11 days of the cool thermal plume created by the experiment reported in this study. By 15 December and until the end of the injection, and during the recovery period reported in this dataset, DTS temperatures recorded at the GU depth in both boreholes, GGA07 and GGA08, were similar, suggesting a uniform distribution of the thermal plume between the two boreholes at Site 3.

Electrical Resistivity Tomography

Figure 6a shows the results of the baseline electrical resistivity inversion between the boreholes at sites 1 (GGA01 – injection borehole and GGA02) and 3 (GGA07 – abstraction borehole and GGA08) (Fig. 1). These were inverted from linearly detrended and averaged data from the ten days prior to the start of the injection. The models correspond closely to the drillers' logs from the construction phase, also shown in Figure 6a. Higher resistivity bands correlated with medium- to coarse-grained sandstones, while more conductive (less resistive) zones are recovered at the depth of the Glasgow Upper mine working. A near-borehole higher resistivity domain is apparent around GGA02 at the depth of the Glasgow Upper mine working, where the grout plug is located.

Typically, electrical conductivity of groundwater increases by approximately 2% per 1°C temperature variation (increase) (Hayley *et al.* 2007). Conversely, for small changes, resistivity will decrease by ~2% per °C temperature increase. The time-lapse resistivity sections (Fig. 6b) show the relative change of resistivity at selected times during the experiment. The 2% change contour is shown for reference. Maximum changes of almost 10% were observed in the resistivity images near the injection borehole, however the 2% per °C conversion must be taken with caution and avoid direct application for the estimation of temperatures because (1) there is some uncertainty in the value of the coefficient and its variability in saturated media for various geological materials (Ma *et al.* 2011) and, (2) there is also uncertainty in the resistivity images caused by both the measurement noise and the geophysical inversion procedure. Therefore, until further calibration and laboratory estimates of the coefficients for the Glasgow site materials, the relationship must be taken with caution. Nevertheless, the results are consistent with the hypothesis of a change in resistivity caused by the temperature change and they provide new information about the spatial and temporal scales of the thermal changes.

The time lapse sequence for site 1, between GGA01 and GGA02, initially shows the resistivity change concentrated at the GU interval in GGA01, but after 3 days it had extended beyond GGA02. At the end of the experiment, changes of more than 10% were observed in the GU mine working interval. At this time, the effect of temperature change along the rock mass around the borehole was starting to be visible. The progressive effect and development of the thermal influence via heat conduction around the borehole and above and below the mine workings is shown as a widening of the resistivity change area over time. A vertical region of low change (white) around the electrodes in GGA02 at the GU mine working depth (about 48 mbgl) showed the effect of the grout plug and it could be observed how with time the resistivity changed progressively as heat via conduction penetrated through this volume (in accordance with the observations in the GGA02 DTS, Fig. 5). At the end of the injection a temperature change of at least 1°C could be observed in the bedrock up to around 42–43 mbgl between GGA01 and GGA02, indicating a thermally affected zone of about 5 m above the mine workings. This could have been produced by heat conduction but also enhanced by potential fracturing of the sandstone at the roof of the mine working. The thermal effect of the injection of cooler water into the mine workings and in the bedrock was still noticeable 7 days after the end of the injection, although of smaller magnitude than at the end of the injection, and at the end of the recovery period.

Discussion and conclusion

Multiphysical monitoring of the thermal plume

The combination of monitoring techniques has allowed the direct and indirect measurement of the temperature changes caused by the experiment during the abstraction–reinjection phase and during the early stage of recovery. This is, to the best of our knowledge, the first time that this multiphysical approach has been applied with this level of detail to geothermal experimentation in flooded mines. The integration of the results provided information to develop a general understanding of the processes that occurred during the experiment.

The injection started on 28 November, with abstraction and reinjection at 6 l s^{-1} from GGA07 to GGA01, respectively. The initial water temperature abstracted from GGA07 measured by the wellhead and the downhole logger was about 11.95 and 11.8°C, respectively, due to the relative location of both sensors and potentially circulation effects in the borehole.

In GGA01, the injection of cooler water resulted in the cooling of a volume of rock around the cased section of the borehole which evolved with variable rate as shown on the DTS data (Fig. 5). DTS near-borehole measurements do not provide information of the extent or penetration of heat transfer through the rock but inform one

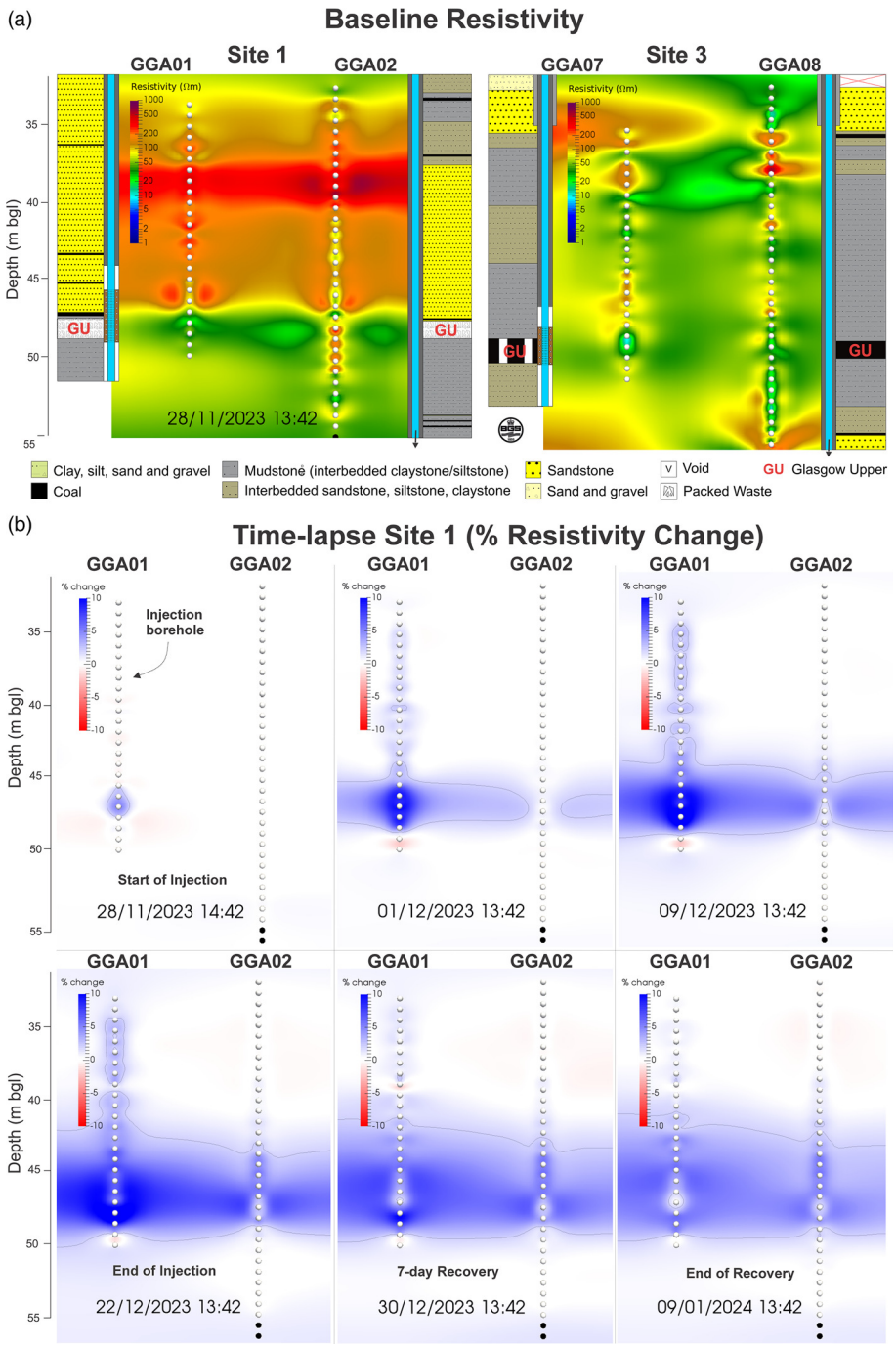

Fig. 6. (**a**) Baseline resistivity inversion from sites 1 and 3. (**b**) Time-lapse electrical resistivity changes (in %) related with the injection of cooler water in GGA01 and the development of the thermal plume in site 1. Contours show the 2% electrical resistivity change.

of the decay temperature curves that are related with the cooler water and the thermal properties of the rock strata nearby.

The main mechanism of heat transfer was the thermal cool plume developed from the screened interval of GGA01 into the mine workings driven by the flow of water through this more permeable part of the reservoir. The DTS showed that the plume flowed out from the borehole through the screened interval almost instantaneously. The extent of the advective cool plume could be tracked with ERT data that show how it extended progressively to pass GGA02 after 2 days (possibly earlier), located at 10 m distance from the injection borehole. The arrival of the thermal plume at GGA02 can also be observed after approximately 3 days in the DTS data (Fig. 5). However, due to the grout plug used to seal the mine working and the lack of direct contact with the mine water it would mean that this temperature signal is interpreted to result from both advection in the flooded mine working of loosely packed waste, plus conduction of the thermal signal through the grout plug, therefore the arrival time must have been earlier than could be detected by the DTS in this type of well completion. This highlights the importance of understanding where exactly the DTS cable is located and what are the backfill materials, thicknesses and well construction details, when comparing data from multiple wells. The grout plug was identified as a blank vertical stripe on the ERT inversions, corresponding to a borehole volume that is unaffected at the initial stages by the temperature change. The cool plume would progressively develop towards the abstraction borehole driven by groundwater flow in the most transmissive parts of the mine water reservoir towards the abstraction borehole GGA07. The arrival of the thermal plume to the abstraction borehole GGA07, located at 135 m from the injection borehole GGA01, was interpreted from information across multiple monitoring technologies as being marked by small temperature changes of less than 0.15°C, in comparison to the 3–4°C induced at the injection borehole. Across the multiple techniques, after 10 days of the experiment, a decrease

in the measured temperature would suggest the arrival of the plume of cooler mine water. Both the downhole hydrogeological logger and thermal sensor at the wellhead in the abstraction borehole, measured a change in the temperature trend, with a temperature decrease of around 0.1°C by the end of the experiment (Fig. 2). This is, however, partially masked by a previous gradual increase of the abstraction temperature, that could have been caused by an earlier heat injection experiment that finished in October 2023 (Gonzalez Quiros *et al.* 2025) from which remnant heat is shown in the pre-experiment vertical profiles in the injection borehole GG01 (Fig. 4b). A very similar behaviour was observed in the DTS cable of GGA07 at the depth of the GU screened interval (Fig. 4c).

The effect of the cooling extended above and, to a lesser extent, below the mine workings at later times, as shown in the ERT inversions (Fig. 6) and on the DTS temperature profile (Fig. 4b; Fig. 5). A thermally affected zone with temperature depleted by more than 1°C was observed up to 5 m above the mine workings between GGA01 and GGA02, this being the effect of heat conduction, and, potentially, of advective flow in the fractured roof above the mine workings. A limited extent of 1–2 m of fractured rock above the mine workings have been directly observed at the Observatory (Monaghan *et al.* 2022). Pressure responses in previous pumping tests in the nearby borehole GGA03r (Gonzalez Quiros *et al.* 2024) located 20 m away from GGA01 and screened in the bedrock *c.* 9 m above the mine workings would also suggest some hydraulic communication between the bedrock and the mine aquifer, and, potentially, a more pervasive fracturing. However, pressure changes were not clearly observed in GGA03r during this experiment, potentially as a result of the combined effect of the abstraction and reinjection boreholes within the same mine working.

Advances and challenges in multiphysical thermal monitoring

The integration of multiphysical techniques presented in this work has provided a unique perspective of the development and evolution of the thermal plume. Even when changes were small and close to the limits of detectability of the sensors, this work has shown that the thermal changes induced by the heat abstraction (cooling) experiment such as the one presented here can be tracked with the array of multiphysical instrumentation available at the Glasgow Observatory.

Distributed temperature sensing is being more widely used in geothermal applications, but various configurations and installations have been reported in the literature, including inside (e.g. Schölderle *et al.* 2021) and outside (less common for open-loop operations, e.g. Reinsch *et al.* 2013) of the borehole casing. The utility and practicality of either varies, while the in-hole installation is less sensitive to lithological impacts, it can provide information of the fluid temperature, especially for long boreholes/screened intervals, to evaluate well circulation and identify the main zones of abstraction/injection (Patterson *et al.* 2017). On the other hand, the installation outside the casing is more sensitive to conductive processes and can be used to estimate the thermal properties of the host rocks (Receveur *et al.* 2026). This approach has been shown to provide good results to evaluate the performance and characterize borehole heat exchangers in combination with thermal response tests (known as advanced or distributed thermal response tests) (Wilke *et al.* 2020). This information can be very useful in closed-loop systems to inform estimates of potential and rates of thermal exchange and storage (Kvalsvik *et al.* 2025). It has also been used to identify constructive defects (Iten *et al.* 2024). A limitation with an installation on the outside of the casing can be found if the cable has been damaged after installation, as the cable cannot be (or is difficult and very expensive) retrieved if there is a failure.

ERT provides information on the penetration and extent of the thermal plume in the rock mass and the mine working, but the spatial resolution of the technique decreases with distance from the electrodes, and the inversion process typically applies a smoothness constraint of some degree (Binley and Slater 2020). Therefore, providing exact estimates of extent and magnitude of the thermal impact is difficult. Installation of ERT is not as straightforward and more expensive than DTS. The data processing, inversion and interpretation is also more complex; however, automated systems are making great progress in delivering meaningful results to the end-user.

The value added by combining the capabilities of both DTS and ERT with the various sensors and downhole loggers is the ability to measure temperature changes on a wider volume, and to image the volume of influence of the thermal disturbance, especially difficult for the conductive heat transport in the bedrock at the field scale. Using the DTS it would be possible to constrain the thermal properties of the injection and recovery measured curves at various depths associated with the lithological variations, while the ERT can be used to constrain the depth of penetration of the thermal front.

Coupled or joint multiphysical modelling and inversion (e.g. González-Quirós and Comte 2021) can be developed to constrain some of the uncertainties derived from the lower resolution of the geophysical methods. By modelling the flow and heat transport processes, and including the adequate petrophysical relationships, it would be possible to reproduce the electrical response measured by the ERT.

Implications for geothermal and thermal energy storage

Design of mine water geothermal systems and their long-term sustainability rely on a good characterization of the mine aquifer. One of the key challenges for heat abstraction operation is the location of the boreholes that must target productive zones of the mine to operate at the required flow rates and, at the same time, avoid thermal feedback (i.e. abstraction of reinjected water before it has had time to recover its temperature). In contrast, mine thermal energy storage projects may wish to use boreholes with interactions, with knowledge of the rate of heat dissipation and recovery vitally important.

This work has shown how in a highly transmissive (estimated hydraulic conductivity of *c.* 1000 m/d; Shorter *et al.* 2021) level of mine workings, a thermal cool plume generated and induced by a relatively low flow rate, 6 l s^{-1}, passed the GGA02 borehole located 10 m away in less than 2 days, and interpreted to have reached the abstraction borehole located at 135 m away in 10 days, although with a very small gradual temperature fall. This interpretation was made on the basis of a previous heat injection experiment at the Observatory with the same configuration of boreholes but 12 l s^{-1} flow rate, in which thermal breakthrough was observed at GGA07 after less than 5 days (Gonzalez Quiros *et al.* 2025).

These results quantify the well-known 'rule' that for geothermal heat abstraction operations should avoid locating both abstraction and reinjection boreholes at close distance in the same level of hydraulically connected mine workings, to avoid thermal breakthrough and homogenization of the resource. Under similar types of connected mine workings with high transmissivity this would mean hundreds of metres apart, which would not be viable for small operations, although could be considered for large district heating networks. Alternative designs with the abstraction and reinjection boreholes targeting different levels of mine workings have been successfully developed in the UK (Banks *et al.* 2022) or the Netherlands (Verhoeven *et al.* 2014). The relatively short timescales for thermal plume development observed during this experiment reinforces points made by Banks *et al.* (2022) that the variability of

mine working types and hydraulic properties require specific site assessment with the development of an appropriate conceptual hydrogeological model and hydrogeological investigations, including well testing.

The results also show that the effect of geothermal operation is not only constrained to the level of mine workings. The multi-physical monitoring, especially ERT, has shown that the effect of the cool thermal plume extends some metres above the mine workings, this due to either heat conduction, the effect of fracturing, or both. The electrical resistivity tomography provided a spatially more extensive imaging of the plume development and allowed to observed the extent of the thermally affected zone, with more than 1°C temperature change on a volume of radius of less than 1 m around the cased section of the injection borehole but up to 5 m above the mine workings, which constituted the preferential flow path for the cooled water. The DTS provided information on the rates of cooling and recovery and showed the direct relationship with lithological variations for the conductive heat transfer, with faster cooling at the clay and mudstone levels and slower at the sandstone. In the abstraction well a small temperature decrease was observed in both the downhole logger and the wellhead sensors after 10 days. The same trends were measured and observed in the DTS and ERT around the injection borehole where the thermal plume could be seen to spread rapidly under flow rates of 6 l s^{-1} and ΔT of 3–4°C. This has direct influence on geothermal potential assessments, that sometimes are based on volumetric estimations accounting only for the mined volume, and on the sustainability of the system. In addition, these are important considerations for the potential use of flooded mines for thermal energy storage. First, because it has been demonstrated that the available volume for thermal storage is larger than the mine voids themselves, and secondly, because the injected heat (or cool in this experiment) would remain for long periods of time providing a very favourable scenario for seasonal thermal storage.

To conclude, quantifying the rates and magnitudes of heat flow processes provides data to feed into feasibility studies and models for the sustainability and efficiency of mine water heat and storage projects for heating and cooling of buildings. The results and insights presented in this work can be used by designers for planning of geothermal systems and by regulators, especially for permitting and managing of mine water blocks. This experiment has shown how multiple factors (hydraulic and thermal properties, borehole configuration, operational parameters, etc.) control the rate and magnitude of the processes of heat transport in flooded mines. Further evaluation is necessary on the recovery efficiency of very transmissive mines and the more appropriate design and operation, accounting for the additional heat stored in the bedrock and the different rates of heat transfer in the system.

Scientific editing by Matthijs Bonte; David Birks

Acknowledgements Many thanks to David Walls and an anonymous reviewer for their thoughtful scientific review, and to the Geological Society editorial team. Calum Ritchie is thanked for illustrating Figure 1. This paper is published with permission of the Executive Director of BGS.

Author contributions **AGQ**: conceptualization (lead), data curation (equal), formal analysis (equal), investigation (equal), methodology (equal), visualization (equal), writing – original draft (lead), writing – review & editing (equal); **AM**: conceptualization (equal), data curation (equal), formal analysis (lead), funding acquisition (lead), methodology (equal), project administration (lead), supervision (lead), visualization (equal), writing – review & editing (equal); **MR**: conceptualization (equal), data curation (equal), formal analysis (equal), investigation (equal), methodology (equal), software (equal), visualization (equal), writing – review & editing (equal); **PW**: conceptualization (equal), data curation (equal), formal analysis (equal), investigation (equal), methodology (equal), resources (equal), software (lead), visualization (lead), writing – review & editing (equal); **DB**: formal analysis (equal), methodology (equal), resources (equal), software (equal), writing – review & editing (equal); **KW-V**: data curation (lead), formal analysis (supporting), methodology (equal), resources (equal), writing – review & editing (supporting); **VS**: conceptualization (supporting), formal analysis (supporting), funding acquisition (lead), project administration (lead), supervision (lead), writing – review & editing (equal); **DJM**: conceptualization (equal), data curation (equal), formal analysis (supporting), investigation (supporting), methodology (supporting), writing – review & editing (equal); **OK**: funding acquisition (equal), investigation (equal), methodology (equal), resources (supporting), supervision (equal), visualization (supporting), writing – review & editing (supporting).

Funding This work was funded by the Natural Environment Research Council (National Capability Funding).

Competing interests All authors are employed by BGS. The authors declare that there is no conflict of interest.

Data availability The datasets generated during and/or analysed during the current study are available in the BGS repository, and will be available from the UKGEOS website (https://www.ukgeos.ac.uk/glasgow/resources-and-data).

References

Banks, D., Steven, J., Black, A. and Naismith, J. 2022. Conceptual modelling of two large-scale mine water geothermal energy schemes: felling, Gateshead, UK. *International Journal of Environmental Research and Public Health*, **19**, 1643, https://doi.org/10.3390/ijerph19031643

Binley, A. and Slater, L.D. 2020. *Resistivity and Induced Polarization: Theory and Applications to the Near-Surface Earth*. Cambridge University Press, Cambridge, UK.

Binley, A., Hubbard, S.S., Huisman, J.A., Revil, A., Robinson, D.A., Singha, K. and Slater, L.D. 2015. The emergence of hydrogeophysics for improved understanding of subsurface processes over multiple scales. *Water Resources Research*, **51**, 3837–3866, https://doi.org/10.1002/2015WR017016

Bloemendal, M., Olsthoorn, T. and Boons, F. 2014. How to achieve optimal and sustainable use of the subsurface for Aquifer Thermal Energy Storage. *Energy Policy*, **66**, 104–114, https://doi.org/10.1016/j.enpol.2013.11.034

Cai, W., Wang, F. *et al.* 2021. Analysis of heat extraction performance and long-term sustainability for multiple deep borehole heat exchanger array: a project-based study. *Applied Energy*, **289**, 116590, https://doi.org/10.1016/j.apenergy.2021.116590

Chu, Z., Dong, K., Gao, P., Wang, Y. and Sun, Q. 2021. Mine-oriented low-enthalpy geothermal exploitation: a review from spatio-temporal perspective. *Energy Conversion and Management*, **237**, 114123, https://doi.org/10.1016/j.enconman.2021.114123

Ciriaco, A.E., Zarrouk, S.J. and Zakeri, G. 2020. Geothermal resource and reserve assessment methodology: overview, analysis and future directions. *Renewable and Sustainable Energy Reviews*, **119**, 109515, https://doi.org/10.1016/j.rser.2019.109515

Comte, J.C., Wilson, C., Ofterdinger, U. and González-Quirós, A. 2017. Effect of volcanic dykes on coastal groundwater flow and saltwater intrusion: a field-scale multiphysics approach and parameter evaluation. *Water Resources Research*, **53**, 2171–2198, https://doi.org/10.1002/2016WR019480

Fadel, M., Reinecker, J., Bruss, D. and Moeck, I. 2022. Causes of a premature thermal breakthrough of a hydrothermal project in Germany. *Geothermics*, **105**, 102523, https://doi.org/10.1016/j.geothermics.2022.102523

González-Quirós, A. and Comte, J.C. 2021. Hydrogeophysical model calibration and uncertainty analysis via full integration of PEST/PEST++ and COMSOL. *Environmental Modelling & Software*, **145**, 105183, https://doi.org/10.1016/j.envsoft.2021.105183

Gonzalez Quiros, A., MacAllister, D.J. *et al.* 2024. De-risking green energy from mine waters by developing a robust hydrogeological conceptual model of the UK Geoenergy Observatory in Glasgow. *Hydrogeology Journal*, **32**, 1307–1329, https://doi.org/10.1007/s10040-024-02778-y

Gonzalez Quiros, A., Receveur, M., Monaghan, A., Starcher, V., Walker-Verkuil, K. and van Hunen, J. 2025. Influence of mine geometry and working type on groundwater flow and heat transport for geothermal exploitation. *In:* Valente, T., Mühlbauer, R., Ordóñez, A. and Wolkersdorfer, C. (eds) *International Mine Water Association Conference 2025 - Time to Come*. International Mine Water Association, 377–382.

Hahn, F. 2024. *Geothermal Reutilization of an Abandoned Colliery Coupled with a District Heating Grid and a High-Temperature Underground Storage*. PhD dissertation, Ruhr-Universität Bochum, https://doi.org/10.13154/294-12371

Hall, I.H.S., Browne, M.A.E. and Forsyth, I.H. 1998. *Geology of the Glasgow District: Memoir for 1:50,000 Geological Sheet 30E (Scotland)*. British Geological Survey, Keyworth, UK.

Hayley, K., Bentley, L.R., Gharibi, M. and Nightingale, M. 2007. Low temperature dependence of electrical resistivity: implications for near surface geophysical monitoring. *Geophysical Research Letters*, **34**, L18402, https://doi.org/10.1029/2007GL031124

Holmes, J., Chambers, J. *et al.* 2020. Four-dimensional electrical resistivity tomography for continuous, near-real-time monitoring of a landslide affecting transport infrastructure in British Columbia, Canada. *Near Surface Geophysics*, **18**, 337–351, https://doi.org/10.1002/nsg.12102

Iten, M., Bühler, M., Fischli, F., Bethmann, F. and El-Alfy, A. 2024. Distributed fiber-optic temperature monitoring in boreholes of a seasonal geothermal energy storage. *Procedia Structural Integrity*, **64**, 1642–1648, https://doi.org/10.1016/j.prostr.2024.09.420

Jardón, S., Ordóñez, A., Álvarez, R., Cienfuegos, P. and Loredo, J. 2013. Mine water for energy and water supply in the Central Coal Basin of Asturias (Spain). *Mine Water and the Environment*, **32**, 139–151, https://doi.org/10.1007/s10230-013-0224-x

Jessop, A.M., MacDonald, J.K. and Spence, H. 1995. Clean energy from abandoned mines at Springhill, Nova Scotia. *Energy Sources*, **17**, 93–106, https://doi.org/10.1080/00908319508946072

Kvalsvik, K.H., Ramstad, R.K., Holmberg, H. and Kocbach, J. 2025. Measurements and simulations of high temperature borehole thermal energy storage in Drammen, Norway-evaluation of thermal losses and thermal barrier. *Geothermics*, **125**, 103192, https://doi.org/10.1016/j.geothermics.2024.103192

LaBrecque, D.J. and Yang, X. 2001. Difference inversion of ERT data: a fast inversion method for 3-D in situ monitoring. *Journal of Environmental & Engineering Geophysics*, **6**, 83–89, https://doi.org/10.4133/JEEG6.2.83

Lesparre, N., Robert, T., Nguyen, F., Boyle, A. and Hermans, T. 2019. 4D electrical resistivity tomography (ERT) for aquifer thermal energy storage monitoring. *Geothermics*, **77**, 368–382, https://doi.org/10.1016/j.geothermics.2018.10.011

Ma, R., McBratney, A., Whelan, B., Minasny, B. and Short, M. 2011. Comparing temperature correction models for soil electrical conductivity measurement. *Precision Agriculture*, **12**, 55–66, https://doi.org/10.1007/s11119-009-9156-7

Monaghan, A.A., Barron, H.F., Starcher, V., Shorter, K.M. and Walker-Verkuil, K. 2020*a*. *Mine Water Characterisation and Monitoring Borehole GGA01, UK Geoenergy Observatory, Glasgow*. British Geological Survey, Nottingham, UK.

Monaghan, A.A., Starcher, V., Barron, H.F., Shorter, K.M. and Walker-Verkuil, K. 2020*b*. *Borehole GGA02, UK Geoenergy Observatory, Glasgow*. British Geological Survey, Nottingham, UK.

Monaghan, A.A., Starcher, V. *et al.* 2022. Drilling into mines for heat: geological synthesis of the UK Geoenergy Observatory in Glasgow and implications for mine water heat resources. *Quarterly Journal of Engineering Geology and Hydrogeology*, **55**, https://doi.org/10.1144/qjegh2021-033

Ó Dochartaigh, B.É., Bonsor, H. and Bricker, S. 2019. Improving understanding of shallow urban groundwater: the Quaternary groundwater system in Glasgow, UK. *Earth and Environmental Science Transactions of the Royal Society of Edinburgh*, **108**, 155–172, https://doi.org/10.1017/S1755691018000385

Patterson, J.R., Cardiff, M., Coleman, T.I., Wang, H.F., Feigl, K.L., Akerley, J. and Spielman, P. 2017. Geothermal reservoir characterization using distributed temperature sensing at Brady Geothermal Field, Nevada. *Geophysics*, **36**, https://doi.org/10.1190/tle36121024a1.1

Receveur, M., Gonzalez Quiros, A., Monaghan, A., Starcher, V., Walker-Verkuil, K., Boon, D. and Van-Hunen, J. 2026. Thermal response of heterolithic deposits in flooded coal mines: implication for heat storage potential. *Geothermics*, **134**, 103525, https://doi.org/10.1016/j.geothermics.2025.103525

Reinsch, T., Henninges, J. and Ásmundsson, R. 2013. Thermal, mechanical and chemical influences on the performance of optical fibres for distributed temperature sensing in a hot geothermal well. *Environmental Earth Sciences*, **70**, 3465–3480, https://doi.org/10.1007/s12665-013-2248-8

Schölderle, F., Lipus, M., Pfrang, D., Reinsch, T., Haberer, S., Einsiedl, F. and Zosseder, K. 2021. Monitoring cold water injections for reservoir characterization using a permanent fiber optic installation in a geothermal production well in the Southern German Molasse Basin. *Geothermal Energy*, **9**, 1–36, https://doi.org/10.1186/s40517-021-00204-0

Shorter, K.M., MacDonald, A.M., O Dochartaigh, B.E., Elsome, J. and Burke, S. 2021. *Data Release and Initial Interpretation of Test Pumping of Boreholes at the Glasgow UK Geoenergy Observatory*. British Geological Survey Open Report, OR/21/016.

Sweeney, A., van Hunen, J., Mouli-Castillo, J. and Gluyas, J. 2025. The need to regulate thermal interference between mine water geothermal systems: a UK perspective. *Quarterly Journal of Engineering Geology and Hydrogeology*, **58**, qjegh2024-185, https://doi.org/10.1144/qjegh2024-185

Verhoeven, R., Willems, E., Harcouët-Menou, V., De Boever, E., Hiddes, L., Op't Veld, P. and Demollin, E. 2014. Minewater 2.0 project in Heerlen the Netherlands: transformation of a geothermal mine water pilot project into a full scale hybrid sustainable energy infrastructure for heating and cooling. *Energy Procedia*, **46**, 58–67, https://doi.org/10.1016/j.egypro.2014.01.158

Walls, D.B., Banks, D., Boyce, A.J. and Burnside, N.M. 2021. A review of the performance of minewater heating and cooling systems. *Energies*, **14**, 6215, https://doi.org/10.3390/en14196215

Wilke, S., Menberg, K., Steger, H. and Blum, P. 2020. Advanced thermal response tests: a review. *Renewable and Sustainable Energy Reviews*, **119**, 109575, https://doi.org/10.1016/j.rser.2019.109575